Double-boson-exchange processes in high-energy $\nu_\mu e^-$ collisions in the standard Weinberg-Salam model

Wang Kong Cheung
Department of Physics, University of Pennsylvania, Philadelphia, Pennsylvania 19104
(Received 2 February 1983)

In this paper, we shall study double-boson-exchange processes in the reactions $\nu_\mu e^- \to \mu^- e^+ e^- \nu_e$, $\nu_\mu e^- \to \mu^+\mu^- e^- \nu_\mu$, and $\nu_\mu e^- \to \mu^+\mu^-\mu^-\nu_e$, using the standard Weinberg-Salam SU(2)$\times$U(1) model of electroweak interactions. At neutrino laboratory energy $\sim$ 100 GeV, the cross section for the first reaction is $\sim 3\times 10^{-44}$ cm^2. This reaction may be observable with experimental facilities in the near future. It could serve as a useful tool for distinguishing the Weinberg-Salam model from other models of electroweak interactions.

I. INTRODUCTION

In this paper we shall study the followng reactions, as examples of double-boson-exchange processes in νe^- scattering[1]:

$$\nu_\mu e^- \to \mu^- e^- W^+ \gamma \to \mu^- e^+ e^- \nu_e \; , \tag{1.1}$$

$$\nu_\mu e^- \to \left\{ \begin{matrix} \mu^- e^- W^+ \gamma \\ e^- Z^0 \nu_\mu \gamma \end{matrix} \right\} \to \mu^+\mu^- e^- \nu_\mu \; , \tag{1.2}$$

$$\nu_\mu e^- \to \mu^- e^- W^+ \gamma \to \mu^+ \mu^- \mu^- \nu_e \; . \tag{1.3}$$

Our calculations are based on the standard Weinberg-Salam SU(2)$\times$U(1) model of electroweak interactions. As is well known, there are alternative models such as left-right-symmetric models,[2] which give similar predictions as the standard model for low-energy single-boson-exchange-type processes[3]:

$$e^+e^- \to \gamma \text{ or } Z^0 \to \mu^+\mu^- \; ,$$

$$\nu_\mu e^- \to \nu_\mu \nu_e W^- \to \mu^- \nu_e \; ,$$

$$\nu_\mu e^- \to e^- Z^0 \nu_\mu \to e^- \nu_\mu \; .$$

Double-boson-exchange-type processes, such as those studied here, may therefore serve as an important tool to distinguish among alternative models of electroweak interactions.[4] We shall find below that these reactions may be observable with experimental facilities in the near future.

We shall be looking at neutrino beam energies of the order of a few hundred GeV, which corresponds to total c.m. energies of the order of $0.5 \sim 1.0$ GeV. Since total c.m. energies are small compared to the mass of the $W^\pm$ boson, m_W, we shall perform our calculations only to first order in the weak coupling constant, $e^2/m_W{}^2$.

Section II lists the relevant Feynman diagrams and amplitudes in our calculations. Section III gives a discussion of our results. We make some concluding remarks in Sec. IV.

II. FEYNMAN DIAGRAMS AND NUMERICAL CALCULATIONS

To first order in the weak coupling constant $e^2/m_W{}^2$, the amplitudes for (1.1)–(1.3) are given by (our spinor notations and γ matrices follow the standard notations of Bjorken and Drell, see Ref. 5)

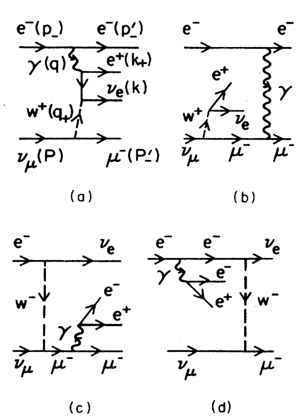

FIG. 1. Feynman diagrams for reaction (1.1).

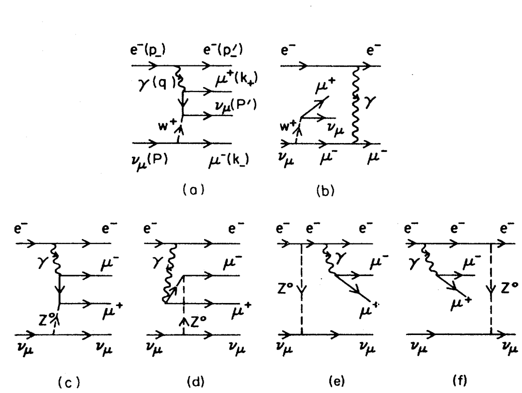

FIG. 2. Feynman diagrams for reactions (1.2).

TABLE I. Behavior of total cross sections for reactions (1.1)—(1.3) as functions of total c.m. energy.

Reaction	Order of magnitude (nb)	Behavior as function of c.m. energy
(1.1) $\nu_\mu e^- \to \mu^- e^+ e^- \nu_e$	10^{-11}—10^{-9}	From $\sqrt{s}=0.3$ to 0.7 GeV, rate of increase with s is more than linear; afterwards, rate is approximately linear.
(1.2) $\nu_\mu e^- \to \mu^+ \mu^- e^- \nu_\mu$	10^{-13}—10^{-9}	Similar behavior as above; nonlinear rate of increase occurs between $\sqrt{s}=0.3$ and 1.4 GeV.
(1.3) $\nu_\mu e^- \to \mu^+ \mu^- \mu^- \nu_e$	10^{-14}—10^{-11}	Similar behavior as above; nonlinear rate of increase occurs between $\sqrt{s}=0.5$ and 1.0 GeV.

$$\begin{aligned}\mathcal{M}_1 &= \mathcal{M}_{1(a)}+\mathcal{M}_{1(b)}+\mathcal{M}_{1(c)}+\mathcal{M}_{1(d)}\\
&= \frac{-e^2g^2}{8m_W{}^2}\Bigg\{\frac{1}{q^2}\bar{u}(p'_-)\gamma^\mu u(p_-)\Bigg[\bar{u}(P'_-)\gamma^\nu(1-\gamma_5)u(P)\bar{u}(k)\gamma_\nu(1-\gamma_5)\frac{1}{\not{q}-\not{k}_+-m_e}\gamma_\mu v(k_+)\\
&\qquad + \bar{u}(k)\gamma^\nu(1-\gamma_5)v(k_+)\bar{u}(P'_-)\gamma_\mu\frac{1}{\not{P}'_- -\not{q}-m_\mu}\gamma_\nu(1-\gamma_5)u(P)\Bigg]\\
&\qquad - \frac{1}{(p'_-+k_+)^2}\bar{u}(p'_-)\gamma^\mu v(k_+)\Bigg[\bar{u}(k)\gamma^\nu(1-\gamma_5)u(p_-)\bar{u}(P'_-)\gamma_\mu\frac{1}{\not{P}'_-+\not{p}'_-+\not{k}_+-m_\mu}\gamma_\nu(1-\gamma_5)u(P)\\
&\qquad + \bar{u}(P'_-)\gamma^\nu(1-\gamma_5)u(P)\bar{u}(k)\gamma_\nu(1-\gamma_5)\frac{1}{\not{p}_- -\not{p}'_- -\not{k}_+ -m_e}\gamma_\mu u(p_-)\Bigg]\Bigg\},\end{aligned} \tag{2.1}$$

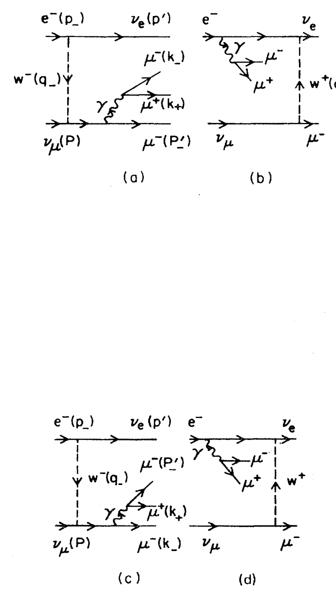

FIG. 3. Feynman diagrams for reaction (1.3).

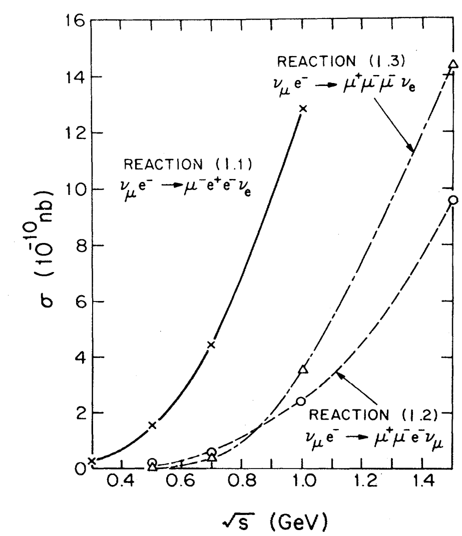

FIG. 4. Total cross sections for reaction (1.1), scale factor $=1$; reaction (1.2), scale factor $=1$; and reaction (1.3), scale factor $=0.01$. Cross sections are in units of nb ($=10^{-33}$ cm^2). To get the actual cross section, the value shown on the graph should be multiplied by the appropriate scale factor.

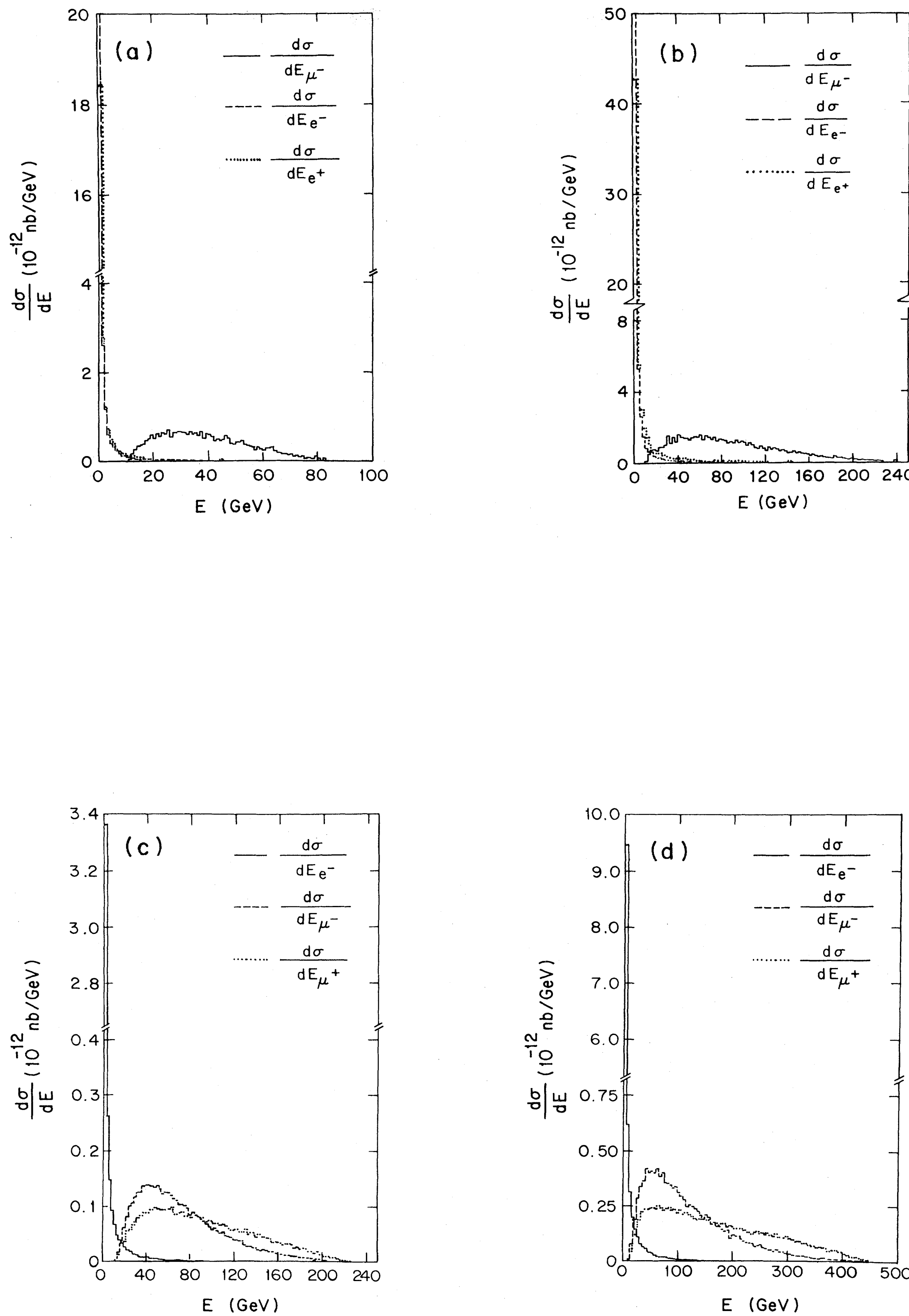

FIG. 5. Differential cross section with respect to E_l, energy of final lepton l ($l = e^+, e^-, \mu^+, \mu^-$), for (a) reaction (1.1), $\sqrt{s} = 0.3$ GeV; (b) reaction (1.1), $\sqrt{s} = 0.5$ GeV; (c) reaction (1.2), $\sqrt{s} = 0.5$ GeV; (d) reaction (1.2), $\sqrt{s} = 0.7$ GeV; (e) reaction (1.3), $\sqrt{s} = 0.5$ GeV; (f) reaction (1.3), $\sqrt{s} = 0.7$ GeV.

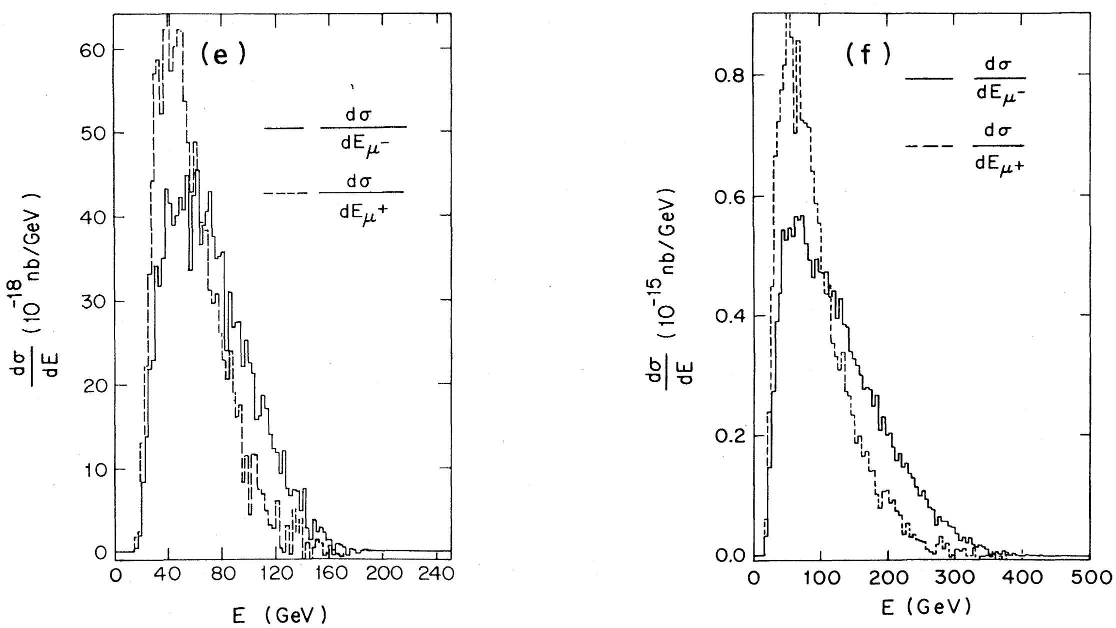

FIG. 5. (*Continued*.)

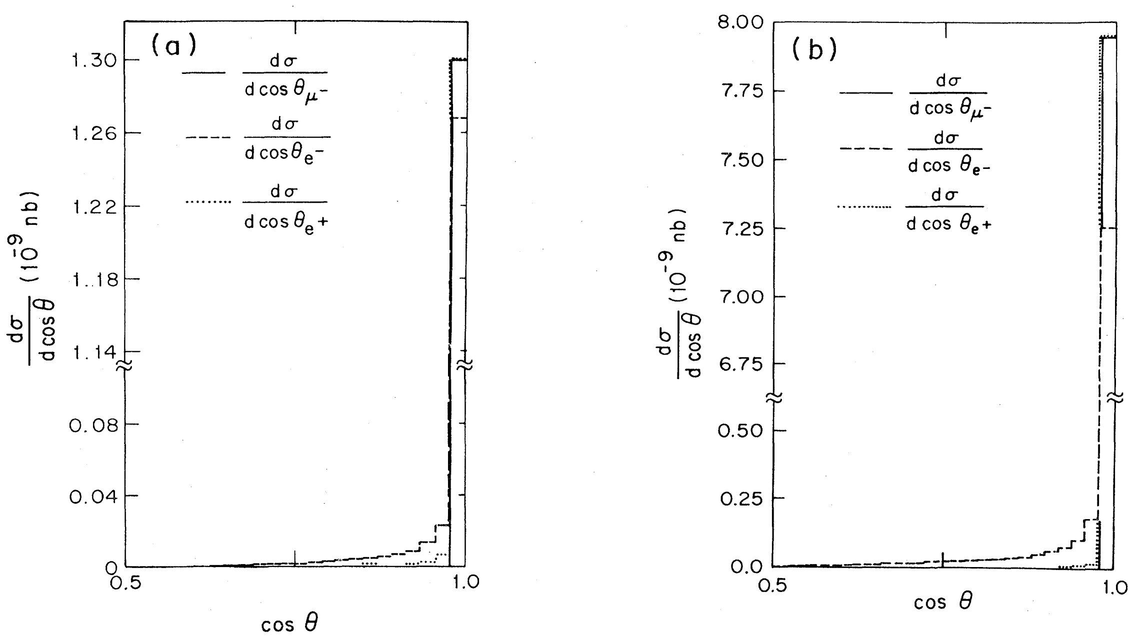

FIG. 6. Differential cross section with respect to $\cos\theta_l$, where θ_l is the angle between the final-lepton l momentum and the initial ν_μ beam ($l=e^+,e^-,\mu^+,\mu^-$), for (a) reaction (1.1), $\sqrt{s}=0.3$ GeV; (b) reaction (1.1), $\sqrt{s}=0.5$ GeV; (c) reaction (1.2), $\sqrt{s}=0.5$ GeV; (d) reaction (1.2), $\sqrt{s}=0.7$ GeV; (e) reaction (1.3), $\sqrt{s}=0.5$ GeV; (f) reaction (1.3), $\sqrt{s}=0.7$ GeV.

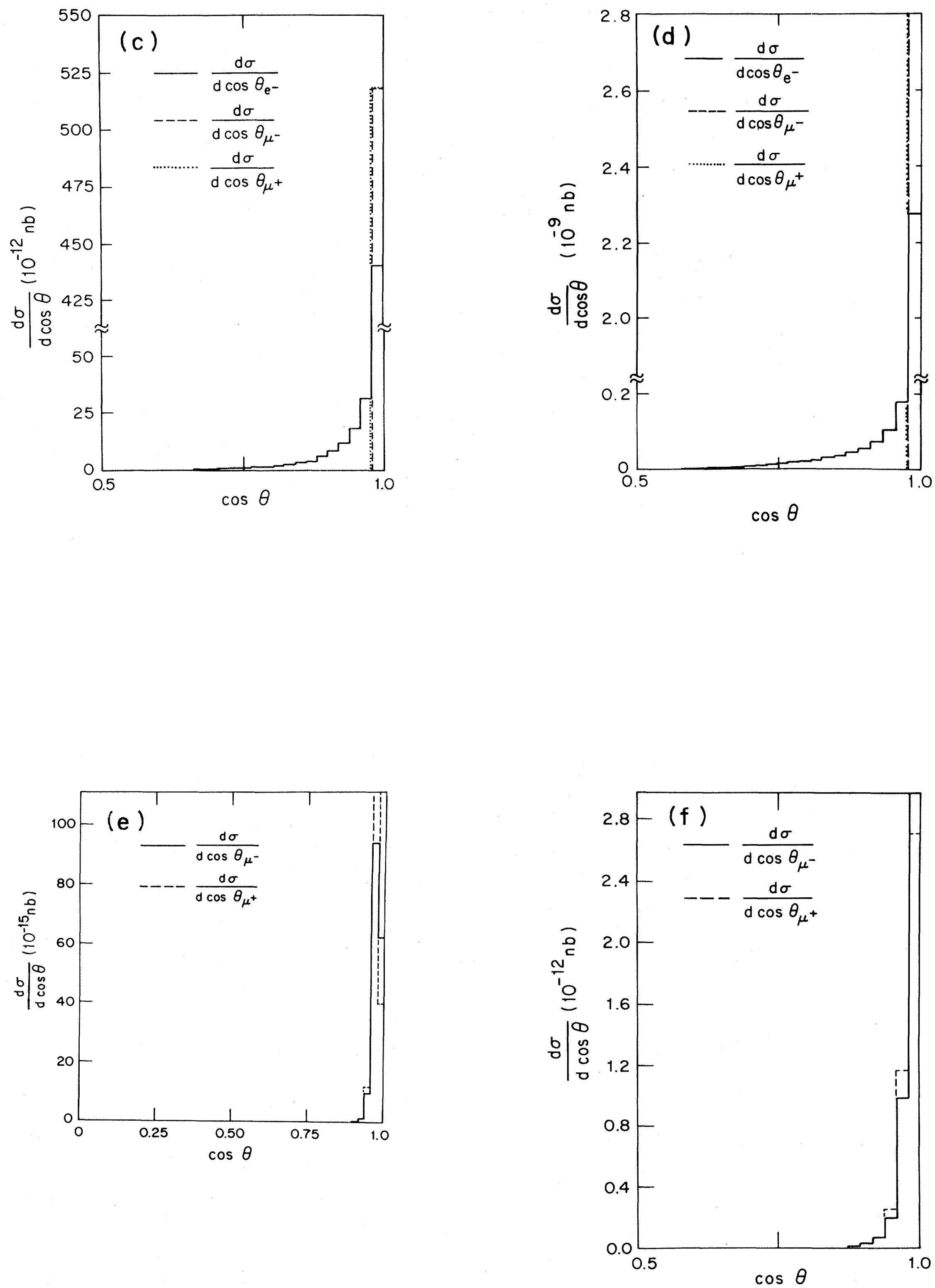

FIG. 6. (*Continued.*)

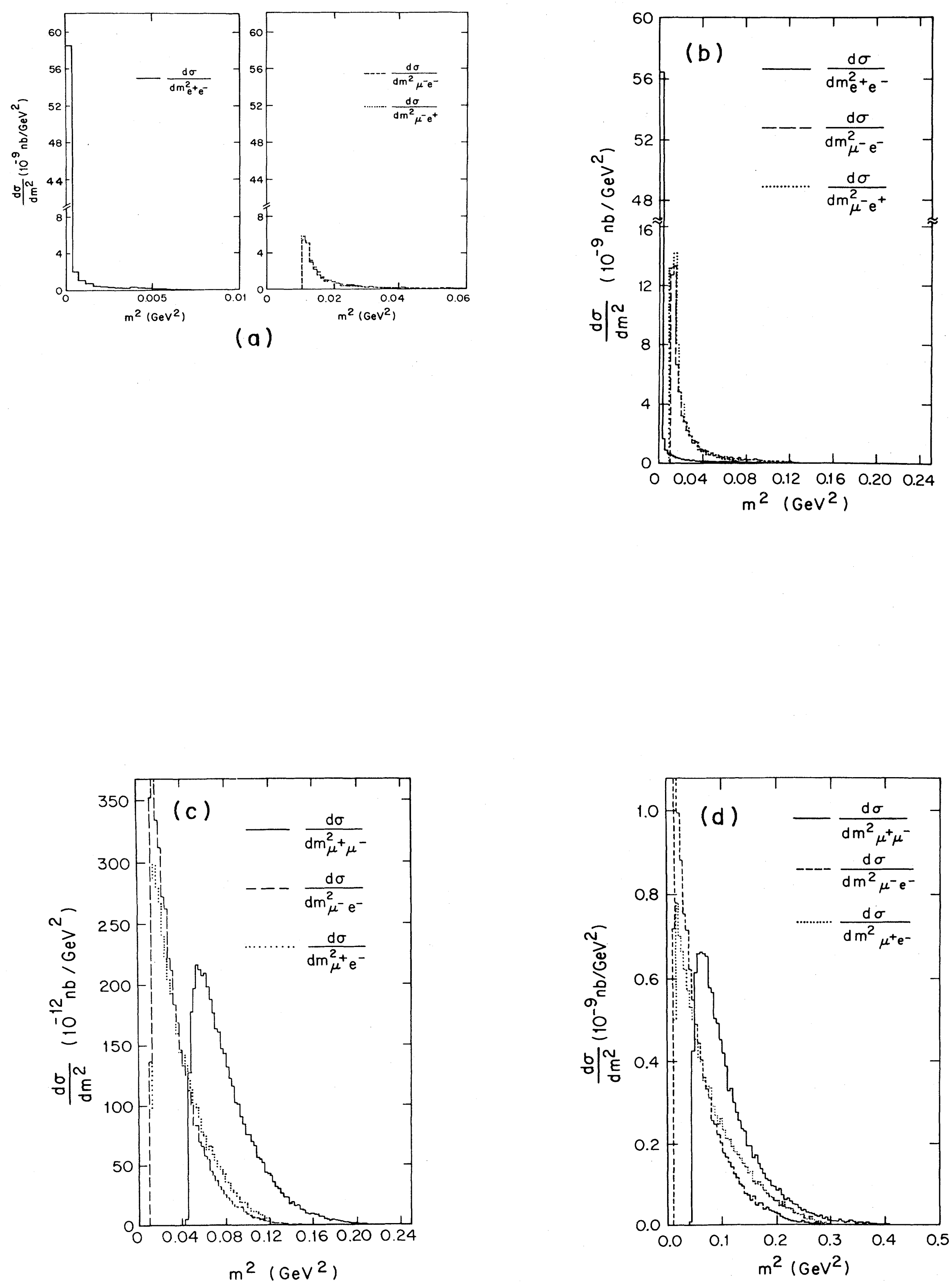

FIG. 7. Differential cross section with respect to $m_{l_1 l_2}{}^2$, squared mass of the lepton pair l_1 and l_2 ($l = e^+, e^-, \mu^+, \mu^-$), for (a) reaction (1.1), $\sqrt{s} = 0.3$ GeV; (b) reaction (1.1), $\sqrt{s} = 0.5$ GeV; (c) reaction (1.2), $\sqrt{s} = 0.5$ GeV; (d) reaction (1.2), $\sqrt{s} = 0.7$ GeV; (e) reaction (1.3), $\sqrt{s} = 0.5$ GeV; (f) reaction (1.3), $\sqrt{s} = 0.7$ GeV.

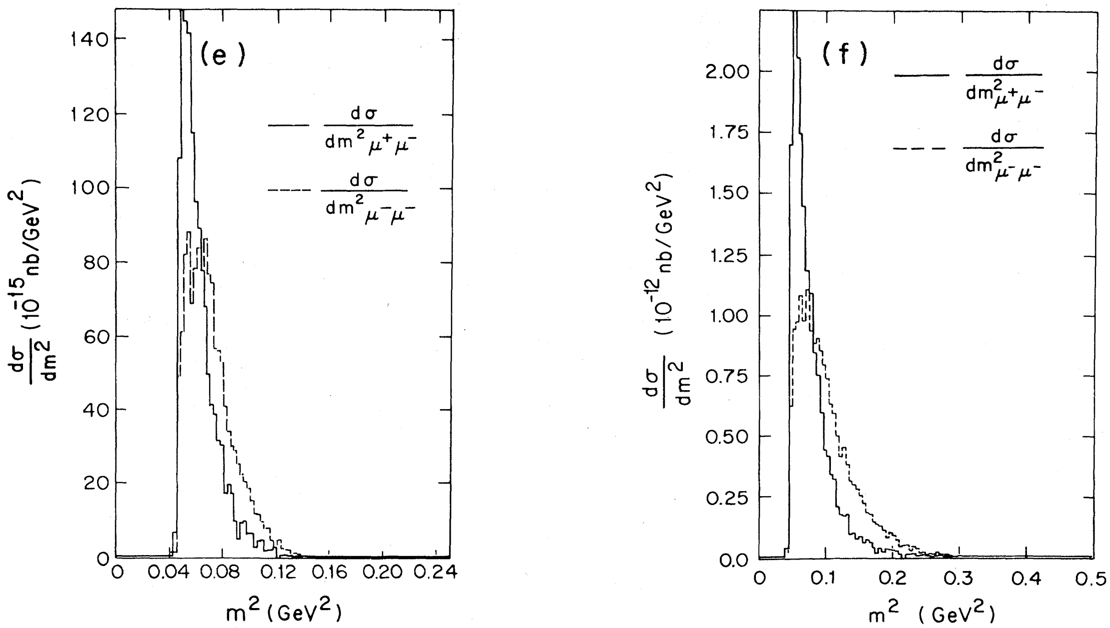

FIG. 7. (*Continued.*)

$$\begin{aligned}
\mathcal{M}_2 &= \mathcal{M}_{2(a)}+\mathcal{M}_{2(b)}+\mathcal{M}_{2(c)}+\mathcal{M}_{2(d)}+\mathcal{M}_{2(e)}+\mathcal{M}_{2(f)} \\
&= -\frac{e^2g^2}{8m_W{}^2q^2}\bar{u}(p'_-)\gamma^\mu u(p_-)\left[\bar{u}(k_-)\gamma^\nu(1-\gamma_5)u(P)\bar{u}(P')\gamma_\nu(1-\gamma_5)\frac{1}{\not{q}-\not{k}_+-m_\mu}\gamma_\mu v(k_+)\right. \\
&\qquad\left.+\bar{u}(P')\gamma^\nu(1-\gamma_5)v(k_+)\bar{u}(k_-)\gamma_\mu\frac{1}{\not{k}-\not{q}-m_\mu}\gamma_\nu(1-\gamma_5)u(P)\right] \\
&\quad -\frac{e^4}{4m_Z^2\sin^2\theta_W\cos^2\theta_W}\frac{1}{q^2}\bar{u}(p'_-)\gamma^\mu u(p_-)\bar{u}(P')\gamma^\nu(1-\gamma_5)u(P) \\
&\quad \times\bar{u}(k_-)\left[\gamma_\mu\frac{1}{\not{k}_--\not{q}-m_\mu}\gamma_\nu(v+a\gamma_5)+\gamma_\nu(v+a\gamma_5)\frac{1}{\not{q}-\not{k}_+-m_\mu}\gamma_\mu\right]v(k_+) \\
&\quad -\frac{e^4}{4m_Z{}^2\sin^2\theta_W\cos^2\theta_W}\frac{1}{(k_-+k_+)^2}\bar{u}(k_-)\gamma^\mu v(k_+)\bar{u}(P')\gamma^\nu(1-\gamma_5)u(P) \\
&\quad \times\bar{u}(p'_-)\left[\gamma_\mu\frac{1}{\not{p}'_-+\not{k}_++\not{k}_--m_e}\gamma_\nu(v+a\gamma_5)+\gamma_\nu(v+a\gamma_5)\frac{1}{\not{p}_--\not{k}_--\not{k}_+-m_e}\gamma_\nu\right]u(p_-)\,,
\end{aligned} \tag{2.2}$$

$$\begin{aligned}
\mathcal{M}_3 &= \mathcal{M}_{3(a)}+\mathcal{M}_{3(b)}+\mathcal{M}_{3(c)}+\mathcal{M}_{3(d)} \\
&= -\frac{e^2g^2}{8m_W{}^2(k_-+k_+)^2}\left[\bar{u}(p')\gamma^\nu(1-\gamma_5)u(p_-)\bar{u}(k_-)\gamma^\mu v(k_+)\bar{u}(P'_-)\gamma_\mu\frac{1}{\not{P}+\not{q}_--m_\mu}\gamma_\nu(1-\gamma_5)u(P)\right. \\
&\qquad\left.+\bar{u}(p')\gamma_\nu(1-\gamma_5)\frac{1}{\not{p}'-\not{q}_+-m_e}\gamma_\mu u(p_-)\bar{u}(P'_-)\gamma^\nu(1-\gamma_5)u(P)\bar{u}(k_-)\gamma^\mu v(k_+)\right] \\
&\quad -\frac{e^2g^2}{8m_W{}^2(P'_-+k_+)^2}\left[\bar{u}(P'_-)\gamma^\mu v(k_+)\bar{u}(p')\gamma^\nu(1-\gamma_5)u(p_-)\bar{u}(k_-)\gamma_\mu\frac{1}{\not{P}+\not{q}_--m_\mu}\gamma_\nu(1-\gamma_5)u(P)\right. \\
&\qquad\left.+\bar{u}(P'_-)\gamma^\mu v(k_+)\bar{u}(k_-)\gamma^\nu(1-\gamma_5)u(P)\bar{u}(p')\gamma_\nu(1-\gamma_5)\frac{1}{\not{p}'-\not{P}+\not{k}_--m_e}\gamma_\mu u(p_-)\right],
\end{aligned} \tag{2.3}$$

TABLE II. Final-particle distributions for reactions (1.1)—(1.3). All final charged particles are concentrated in directions around the initial ν_μ beam.

$\sqrt{s}$ (GeV)	0.3	0.5
E_ν (GeV)	88	245
Reaction (1.1)		
Final μ^- energy spectrum	Broad peak extends from 20—60 GeV, maximum at 30 GeV.	Peak extends from 30—150 GeV, maximum at 60 GeV.
Final e^- energy spectrum	Most e^- have energies below 5 GeV.	Most e^- have energies below 10 GeV.
Final e^+ energy spectrum	Same as above	Same as above.
Distribution with respect to $m_{e^+e^-}{}^2$	Very sharply peaked at values $\lesssim 0.001$ GeV^2.	Very sharply peaked at values $\lesssim 0.005$ GeV^2.
Distribution with respect to $m_{\mu^-e^+}{}^2$, $m_{\mu^-e^+}{}^2$	Peak at ~ 0.01 GeV^2.	Peak at ~ 0.02 GeV^2.
$\sqrt{s}$ (GeV)	0.5	0.7
E_ν (GeV)	245	479
Reaction (1.2)		
Final μ^- energy spectrum	Broad peak extends from 30—100 GeV, maximum at 50 GeV.	Broad peak extends from 30—150 GeV, maximum at ~ 80 GeV.
Final μ^+ energy spectrum	Very broad peak extending from 25—150 GeV, maximum at ~ 70 GeV.	Very broad peak extending from 50—300 GeV, maximum at ~ 100 GeV.
Final e^- energy spectrum	Sharply peaked at values $\lesssim 5$ GeV.	Sharply peaked at values $\lesssim 10$ GeV.
Distribution with respect to $m_{\mu^+\mu^-}{}^2$	Peak extends from 0.05 to 0.10 GeV^2, maximum at 0.07 GeV^2.	Peak extends from 0.06 to 0.14 GeV^2, maximum at 0.08 GeV^2.
Distribution with respect to $m_{\mu^-e^-}{}^2$	Peak extends from 0.02 to 0.04 GeV^2, maximum at ~ 0.03 GeV^2.	Peak extends from 0.025 to 0.07 GeV^2, maximum at ~ 0.03 GeV^2.
Distribution with respect to $m_{\mu^+e^-}{}^2$	Peak extends from 0.02 to 0.06 GeV^2, maximum at ~ 0.03 GeV^2.	Peak extends from 0.025 to 0.10 GeV^2, maximum at ~ 0.03 GeV^2.
Reaction (1.3)		
Final μ^- energy spectrum	Broad peak extends from 30 to 100 GeV, maximum at ~ 60 GeV.	Broad peak extends from 30 to 160 GeV, maximum at ~ 80 GeV.
Final μ^+ energy spectrum	Broad peak extends from 25 to 80 GeV, maximum at ~ 50 GeV.	Broad peak extends from 30 to 110 GeV, maximum at ~ 70 GeV.
Distribution with respect to $m_{\mu^+\mu^-}{}^2$	Sharply peaked at 0.06 GeV^2, extending from ~ 0.05 GeV^2 to ~ 0.07 GeV^2.	Sharply peaked at 0.07 GeV^2, extending from 0.05 to 0.09 GeV^2.
Distribution with respect to $m_{\mu^-\mu^-}{}^2$	Peaked at 0.07 GeV^2, extending from 0.05 to 0.09 GeV^2.	Peaked at 0.08 GeV^2, extending from 0.05 to 0.13 GeV^2.

where $g = e/\sin\theta_W$, $v = 0.25 - \sin^2\theta_W$, and $a = -0.25$ (see Ref. 6). The corresponding Feynman diagrams and the momenta are shown in Figs. 1—3. The cross sections for the reactions (1.1)—(1.3) are calculated by using the Monte Carlo integration program VEGAS.[7]

III. RESULTS AND DISCUSSION

Cross sections for the reactions (1.1)—(1.3) have been calculated for total c.m. energies in the range 0.3—1.5 GeV, which corresponds to laboratory neutrino energies in the range 80—2200 GeV. The behavior of these cross sections as functions of total c.m. energy is shown in Fig. 4. Their features are summarized in Table I.

Distributions with respect to final-particle momenta have been obtained at two c.m. energies: for reaction (1.1), at 0.3 and 0.5 GeV; and for reactions (1.2) and (1.3), at 0.5 and 0.7 GeV, corresponding to neutrino beam energies of 88, 245, and 479 GeV, respectively. These distributions are shown in Figs. 5—7. Table II summarizes the main features of these distributions. We note that all final charged particles are concentrated along the direction of the initial ν_μ beam. At a given energy, the μ^+ and μ^- energy spectra are qualitatively similar for the various reactions. The μ^+ and μ^- take up a large fraction of the ν_μ beam energy. The final e^+ and e^- are emitted with relatively low energies, $\leq$ a few GeV. The squared mass of the muon pairs peaks at $\sim 4m_\mu{}^2$, that of the muon-electron pairs peaks at $\sim m_\mu{}^2$, while that of the e^+e^- pairs peaks at considerably lower values. In these reactions, from an experimental point of view, the muons should be easiest to detect.

IV. CONCLUSION

At neutrino laboratory energies of ~ 100 GeV, cross sections for the reaction $\nu_\mu e^- \to \mu^- e^+ e^- \nu_e$ are $\sim 3\times 10^{-44}$ cm^2. Assuming a neutrino flux of $\sim 10^4$/cm^2/sec, and that the neutrino beam is incident on a target corresponding to $\sim 2\times 10^{32}$ electrons, based on parameters for the neutrino-beam facilities at the Fermilab Tevatron,[8] these cross sections lead to event rates of $\sim 5\times 10^{-3}$ per day. Although these events are not observable with currently available experimental facilities, they are not very far beyond reach. With the proposed alternatives to the standard Weinberg-Salem model of the electroweak interactions, the observation of these events may serve as a useful tool to decide on the correct picture, alternative to the usual single-boson-exchange-type reactions.[9]

ACKNOWLEDGMENTS

I would like to acknowledge the invaluable guidance and helpful discussions of Professor Henry Primakoff through the course of this research, and also useful discussions with Professor Lay-Nam Chang and Professor Alfred Mann. This research was partially supported by the National Science Foundation.

---

[1]Double-boson-exchange processes have been considered within the context of νN scattering; see for example: V. Barger, T. Gottschalk, and R. J. N. Phillips, Phys. Rev. D 18, 2308 (1978); J. Smith, Nucl. Phys. B157, 451 (1979); W. Jager, *ibid.* B142, 273 (1978).

[2]J. C. Pati and A. Salam, Phys. Rev. D 10, 275 (1974); R. N. Mohapatra and J. C. Pati, *ibid.* 11, 566 (1974); R. N. Mohapatra and J. C. Pati, *ibid.* 11, 566 (1974); 11, 2558 (1974); G. Senjanović and R. N. Mohapatra, *ibid.* 12, 1502 (1975); R. N. Mohapatra and G. Senjanović, Phys. Rev. Lett. 44, 912 (1980); Phys. Rev. D 23, 165 (1981).

[3]For a discussion of how predictions of models with two Z bosons compare with the standard Weinberg-Salam models, see Y. Tosa, Phys. Rev. D 26, 1700 (1982), and references therein.

[4]With currently available energies in the e^+e^- machines, it is still difficult to distinguish between models with one Z boson from those with two Z's on the basis of single-boson-exchange processes. Hence it is worth investigating whether double-boson-exchange processes can afford an easier way to distinguish between these two types of models.

[5]J. Bjorken and S. Drell, *Relativistic Quantum Fields* (McGraw-Hill, New York, 1965).

[6]We take the following values for the parameters $\sin^2\theta_W$, and m_Z: $\sin^2\theta_W = 0.23$, $m_Z = 90$ GeV, $m_W = m_Z \cos\theta_W$. See J. E. Kim, P. Langacker, M. Levine, and H. H. Williams, Rev. Mod. Phys. 53, 211 (1981), for a discussion on the values of these parameters.

[7]P. Lepage, Comput. Phys. 27, 555 (1978).

[8]A. K. Mann and R. Stefanski (private communications). The parameters we have assumed for the neutrino beam facilities are as follows: Proton flux $= 10^{12}$ protons/sec, neutrino flux $= 2\times 10^{-6}$ neutrinos/m^2 GeV proton at $E_\nu = 100$ GeV, neutrino energy bin width $=$ 50 GeV, a target of 500 tons of material.

[9]At the neutrino energies considered, ~ 100 GeV, which correspond to c.m. energies ~ 0.3 GeV, the masses of the final particles are significant factors in determining the magnitude of the cross section. The reaction $\nu_\mu e^- \to e^+ e^- e^- \nu_\mu$ is currently under investigation. Its cross section may be much larger than those of the reactions we have studied in this paper, since the masses of the final particles are so much smaller for the former as compared to the latter reactions. Hence the reaction $\nu_\mu e^- \to e^+ e^- e^- \nu_\mu$ may in fact be observable with currently available experimental facilities. The result of our studies on this reaction will be published in a later communication.